LA-UR-77-1877

CONF-770844--1

TITLE: SOME TECHNIQUES FOR DIGITAL PROCESSING, DISPLAY AND INTERPRETATION OF RATIO IMAGES IN MULTISPECTRAL REMOTE SENSING

AUTHOR(S): G. W. Wecksung
J. R. Breedlove

SUBMITTED TO: 1977 International Optical Computing Conference, San Diego, CA

los alamos
scientific laboratory
of the University of California
LOS ALAMOS, NEW MEXICO 87545

An Affirmative Action/Equal Opportunity Employer

Form No. 836
St. No. 2629
1/75

UNITED STATES
ENERGY RESEARCH AND
DEVELOPMENT ADMINISTRATION
CONTRACT W-7405-ENG. 36

SOME TECHNIQUES FOR DIGITAL PROCESSING, DISPLAY AND INTERPRETATION OF RATIO IMAGES IN MULTISPECTRAL REMOTE SENSING*

G. W. Wecksung
J. R. Breedlove, Jr.
University of California
Los Alamos Scientific Laboratory
Los Alamos, New Mexico 87545

Abstract

A simple mathematical interpretation of the properties of ratio images derived from LANDSAT and other sources of multispectral imagery is presented. A spectral signature is defined which is well represented by ratios of pairs of spectral bands and can be related to the problem of clustering and unsupervised learning. Some practical problems arising in the generation of LANDSAT ratio images are considered, and an effective, simple method for reduction of the dynamic range of such images is presented along with digital image processing examples.

Introduction

The technique of ratioing, which consists of forming a new image from a given pair of images by dividing the first given image by the second on a point-by-point basis, was first introduced to digital image processing as a method to detect small color differences in multispectral images of the moon.[1,2] With the widespread availability of LANDSAT digital multispectral imagery, ratioing has been established as a proven tool in geologic investigations.[3-5]

However, it has seemed to us that the value of this approach has been intrinsic in the specific application and that justification in terms of general principles has been lacking. For example, ratioing is a principal tool for geologists, but is not commonly used in crop-monitoring applications. With the four MSS bands of LANDSAT I, we can construct 12 ratio images. Which of these are significant? How does ratioing relate to the problems of supervised and unsupervised learning? These are some of the general problems we consider in this paper.

On the practical side, good ratio images are almost impossible to produce without digital processing. This applies not only to the numerical division performed, but to the necessary preprocessing required, e.g., noise removal, correction for radiometric distortion, geometric rectification, and atmospheric correction. Finally, one perplexing problem which every digital image processor of ratio data must consider is that of dynamic range compression. A ratio of two positive numbers falls in the range between zero and infinity, a range beyond the capacity of any practical image display device. The logarithm and the cube root function are two candidates for a nonlinear contrast stretch function to reduce the dynamic range, but it has been our experience that the effectiveness of these functions as well as the linearly compressed raw ratio is highly scene-dependent and that a great deal of trial and error is required to obtain a satisfactory display. In this paper we consider two of these problems: atmospheric bias correction and dynamic range compression.

The purpose of this paper is not to provide geologic interpretations of ratio images. Rather, we present a mathematical interpretation which provides some insight into classification and clustering problems and which may be of aid to the geologist. We also propose the use of the arctangent as a contrast stretch function to reduce the dynamic range of the ratio data. The choice of this function was directly motivated by the mathematical interpretation. Finally, we present a cursory comparison of various dynamic range compression schemes.

Mathematical Interpretation

Corresponding to each ground resolution element or pixel, a multispectral data acquisition system samples the continuous spectrum of light intensities reflected from that element in a number of spectral bands. Specifically, for the k^{th} of these bands,

$$s_k = \int_0^\infty S(\lambda) R_k(\lambda) d\lambda \quad , \tag{1}$$

where λ is wavelength, $S(\lambda)$ is the captured light spectrum, $R_k(\lambda)$ is the system spectral response function for

*Work performed under the auspices of the Energy Research and Development Administration, Contract No. 7405-ENG-36.

the k^{th} band, and s_k is the k^{th} spectral measurement. In digital systems, s_k is generally quantized into a range of integer values, e.g., 0 to 127; individual values are frequently called DN (digital number).

We consider only systems which are linear or can be made to be linear, so that Equation 1 holds. Figure 1 shows a typical set of response functions for LANDSAT I, a four-band system.[6]

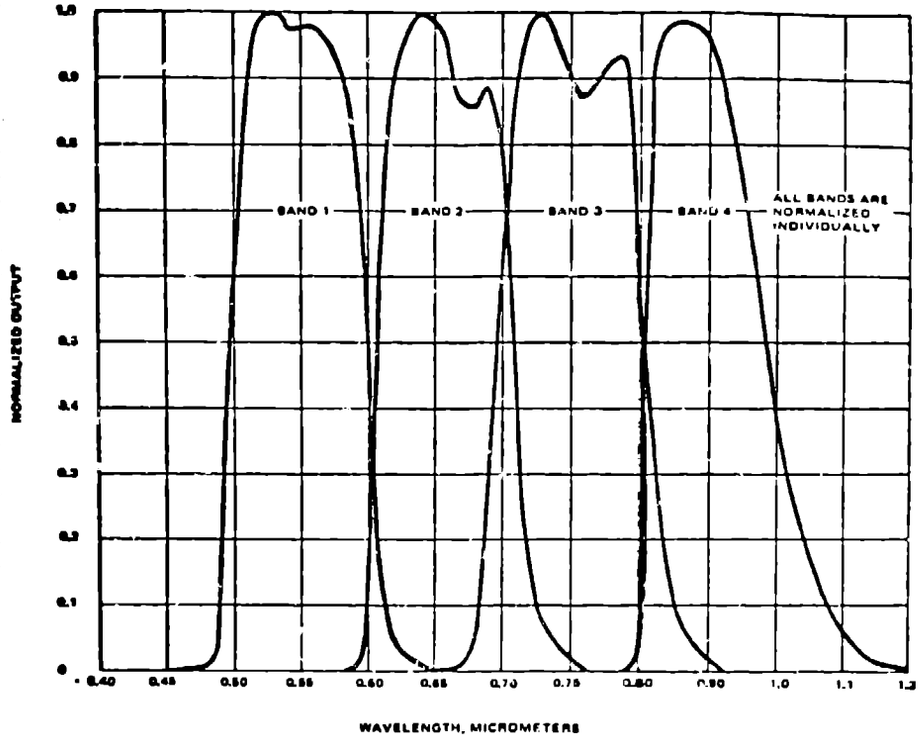

Fig. 1. Typical spectral response functions for LANDSAT I, a four-band system.

Examples of other systems which we might consider range from black and white photography (a one-band system), color photography and the human eye (three-band systems) to 24 (or more)-band airborne systems. Thus, an N-band system acts as a linear operator in which a spectrum, continuous in wave length, is mapped into a N-dimensional spectral measurement vector, as shown in the block diagram in Figure 2.

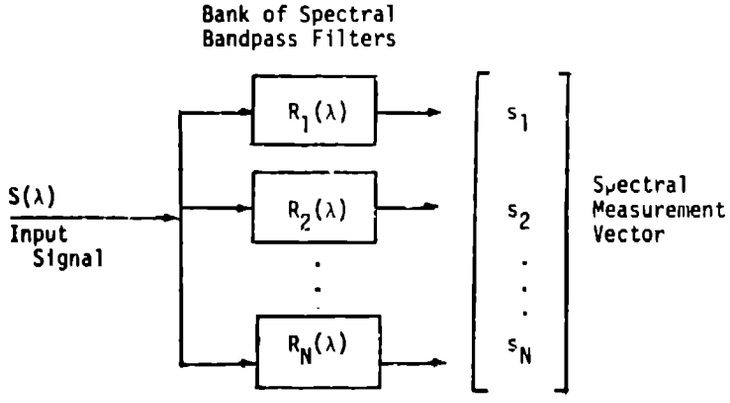

Fig. 2. Block diagram of a linear N-band multispectral data acquisition system.

We observe that we get incomplete spectral information, i.e., given the spectral measurements $s_1, s_2, \ldots, s_N$ and the response functions $R_1(\lambda), R_2(\lambda), \ldots, R_N(\lambda)$, we cannot reconstruct the original spectrum. The best approximation $S^*(\lambda)$ of $S(\lambda)$ knowing only the spectral measurements and the response functions is given by

$$S^*(\lambda) = \sum_{k=1}^{N} c_k R_k(\lambda) \quad , \tag{2}$$

where the constants $c_1, c_2, \ldots c_N$ are solutions to the system of N equations,

$$\sum_{k=1}^{N} \left\{ \int_0^\infty R_j(\lambda) R_k(\lambda) d\lambda \right\} c_k = s_j, \qquad j = 1, \ldots, N, \tag{3}$$

obtained by substituting Equation 2 into Equation 1.[7]

The purpose of the preceding paragraph is to point out that ideally we want to get $S(\lambda)$, but we have to settle for an imperfect representation $S^*(\lambda)$ or most often just the numbers $s_1, s_2, \ldots s_N$, themselves. The latter alternative is often acceptable when the response functions are narrow and nonoverlapping. Indeed, if the response functions were delta-functions located at the centers of the respective spectral bands, then the measurements $s_1, s_2, \ldots s_N$ would trace out the envelope of $S(\lambda)$.

Although the spectral measurement vector may not be a faithful representation of the spectral envelope, its direction and magnitude can always be related, respectively, to the shape and amplitude of the input spectrum for a linear system. For example if $F(\lambda)$ and $S(\lambda)$ are two spectra with the same spectral shape but with different amplitudes, then we can write

$$F(\lambda) = c\, S(\lambda) \quad , \tag{4}$$

where c is a constant. When Equation (4) is substituted into Equation (1), we get the result,

$$\underset{\sim}{f} = c\, \underset{\sim}{s} \quad , \tag{5}$$

where $\underset{\sim}{f}$ and $\underset{\sim}{s}$ are the spectral measurement vectors of $F(\lambda)$ and $S(\lambda)$, respectively.

For a 3-band system, we can plot the vectors $\underset{\sim}{f}$ and $\underset{\sim}{s}$ as points in Figure 3.

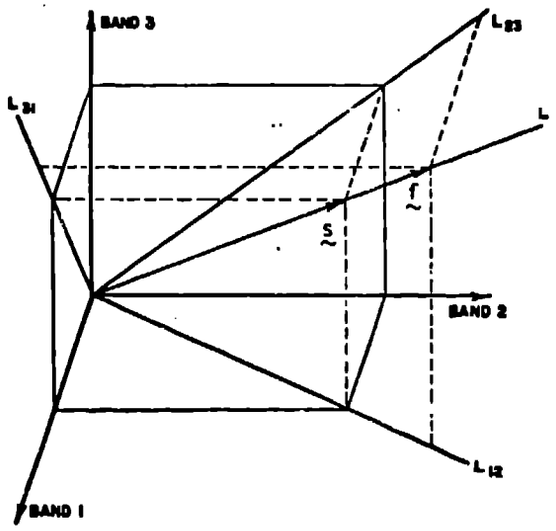

Fig. 3. Spectral space for a 3-band system. The direction of the line L defines a spectral signature corresponding to a class of continuous spectral shapes. The slopes of the lines L_{12}, L_{23}, L_{31}, which are projections of L into the three planes defined by the coordinate axes, determine the direction of L.

Any spectrum with a shape proportional to $S(\lambda)$ will have a measurement vector which also lies on Line L. Since the response functions cannot resolve arbitrary spectra perfectly, there will be other spectra somewhat dissimilar to $S(\lambda)$ which also map onto Line L. If the constant c in equation (4) is greater than unity, f will lie farther from the origin than s. This we can interpret as meaning that f corresponds to a brighter pixel on the multispectral image than $\underset{\sim}{s}$, just as we identify higher DN in a particular band to correspond to brighter values.

If we ignore brightness, the direction of the line L defines a spectral signature corresponding to the input spectral shape. The ratios of all pairs of spectral bands specify this direction, in fact they over-specify it, since they are not independent.

There are many ways of specifying the direction of a line in N-dimensional space, e.g., components of a unit vector, generalized polar coordinates, but all have N-1 degrees of freedom. A choice of N-1 independent ratios of the N coordinates of an arbitrary point on the signature line proves to be a very convenient representation of the direction of the line.

To make this idea more concrete, consider the spectral space corresponding to a 3-band system as shown in Figure 3. The lines L_{12}, L_{23}, and L_{31} are the projections of the signature line L onto the three planes defined by the coordinate axes. The direction of each of these projected lines, in the plane of the projection, can be specified by its slope. If we know the direction of any two of these projected lines, say L_{12} and L_{23}, then we can specify the direction of L. This is evident since L is the intersection of two planes, one defined by the Band-3 axis and L_{12} and the other by the Band-1 axis and L_{23}. Since the slope of either of the projected lines L_{12} or L_{23} is just the ratio of the two coordinates of a typical point on the line, we see that two independent ratios completely specify the direction of the signature line in a 3-band spectral space.

Relation to Clustering and Learning Techniques

Ratioing generally has been regarded as an enhancement procedure rather than a classification procedure, [8] since classification is performed by the geologist who visually interprets the ratio image. One type of material will appear the same or similar in a ratio image regardless of the local topographical slope angle. [3] In other words, spectral measurement vectors corresponding to a homogeneous region with rough topography will vary mainly in brightness and hence they will cluster along the line which we have defined to be the spectral signature of the region.

Evidently, an unsupervised learning approach using classical clustering techniques will not be very effective with this type of data. There would always be the danger of association of darker points on distinct but neighboring lines and disassociation of dark and bright points on the same line. On the other hand, in agricultural applications in which a typical scene consists of fields of crops on a relatively flat terrain, brightness variations should be small and a clustering approach can be considered feasible. If we select a feature space spanned by an independent set of ratios, all points on a signature line in the original spectral space will automatically be grouped into a single class or point in this ratio feature space. Such a space provides the link to a classical clustering approach for geological data.

Due to the poor spectral and spatial resolution of LANDSAT acquired data, dissimilar data can map into the direction of the same signature line and the spectrum corresponding to a given ground resolution element may be a weighted average of several distinct spectra. Hence, it would be difficult to associate a spectrally homogeneous region with a single point in the ratio feature space. The large dynamic range of the ratios can also cause severe spreading problems. We believe that this last problem can be overcome by working with the arctangent of the ratio, which conveys the same information. After classification by ratios or arctangents of ratios, we can always subcluster when albedo differences are important.

It is interesting to note that the spectral signature, as we have defined above, can be related to a supervised learning approach. For example, in discriminant analysis, a sample mean vector and sample covariance matrix are calculated for each of several training sets. Discriminate functions based on these statistics can be designed to assign unknown data vectors to classes of which the training sets are representative. If we assume that sample vectors from a given training set all lie along a straight line in spectral space, we find that the covariance matrix has only one nonzero eigenvalue, and that the signature line goes through the mean vector in the direction of the dominant eigenvalue. [9] Thus, the design of the discriminant functions is highly dependent on the class signature lines.

Atmospheric Correction

In the previous discussion we assumed that the signature line went through the origin of the spectral space. For real data such as LANDSAT, this is not the case due to a scattering contribution from the atmosphere. The captured light spectrum $S(\lambda)$ can be modeled as

$$S(\lambda) = B \cdot G(\lambda) + A(\lambda) \quad , \tag{6}$$

where $A(\lambda)$ is the atmospheric scattering contribution, $G(\lambda)$ is a spectral shape indicative of some material on the ground and B is a brightness factor, or amplitude independent of λ.

We point out that the $B \cdot G(\lambda)$ term can be modeled further in sophisticated ways which consider factors such as solar illumination, atmospheric transmission, bidirectional reflectance, and the surface photometric function.[4] Since many of these factors remain constant or nearly constant over a single LANDSAT frame, we feel justified in the use of the model of Equation (6).

If we regard $G(\lambda)$ and $A(\lambda)$ as being fixed and let B be a parameter, substitution of Equation (6) into Equation (1) results in

$$\underset{\sim}{s} = B \cdot \underset{\sim}{g} + \underset{\sim}{a} \tag{7}$$

where $\underset{\sim}{g}$ and $\underset{\sim}{a}$ denote the spectral measurement vectors obtained by substituting $G(\lambda)$ and $A(\lambda)$ alone for $S(\lambda)$ in Equation (1). Equation (7) is the parametric equation of the spectral signature line corresponding to the spectral shape of $G(\lambda)$ with B as a parameter. For $B = 0$, we have $s = a$. So we may consider the data for a LANDSAT frame to cluster along a family of lines which go through a common point a in the spectral space rather than through the origin. If the atmospheric bias vector a can be estimated, it can be subtracted from s. This is equivalent to shifting the origin of the spectral space to the point a. Clearly, if this correction is not made, points on a signature line will not have a common set of ratios.

The bias vector $\underset{\sim}{a}$ can be estimated, in principle, by a supervised learning technique. If two training sets corresponding to different homogeneous regions in the LANDSAT frame are selected, we can assume that spectral data from a given set clusters along the signature line corresponding to that set. After calculating the sample mean vectors and covariance matrices of the training sets, we can estimate the signature line of a given set, since it goes through the mean vector in the direction of the dominant eigenvector of the covariance matrix. The intersection of the two signature lines then determines the bias vector $\underset{\sim}{a}$. It is desirable to pick a homogeneous training set to include the boundary of a cloud shadow or the sunny and shady sides of a ridge in order to increase the spread of the spectral data vectors along the signature lines.

Some very practical methods for determining the atmospheric bias term are given by Chavez.[10] The DN for the bias term of LANDSAT MSS Band 7 is known empirically to be very close to zero. Points from a single homogeneous training set are selected and plotted one band at a time against Band 7, as shown in Fig. 4. A regression line is then calculated and its intercept of the Band i axis determines the atmospheric bias for Band i. A second method reported by Chavez estimates the atmospheric bias terms from offsets in the histograms of the individual bands. This method is much cheaper to implement and is comparable in accuracy to the first method.

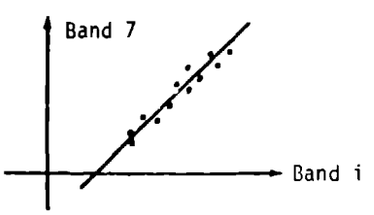

Fig. 4. Determination of the atmospheric bias term for LANDSAT Band i by linear regression.

Dynamic Range Compression - The Angle Image

We have discussed the desirability, in principle, of clustering in a vector space spanned by an independent set of ratios of recorded intensities in pairs of bands in a multispectral imaging system. There are two practical problems in using ratio images. First, ratio images have a dynamic range of $[0, \infty]$; to display a ratio image, the dynamic range must be compressed. Second, the set of data vectors s corresponding to a set of tightly grouped spectral signature lines may not form an obvious cluster in the feature space of ratios. Using the three-dimensional example in Fig. 3, one can see that, for example, if L_{23} is near the Band 2 axis, a large angular displacement corresponds to a small change in the ratio of Band 3 to Band 2. Conversely, for large ratio values, a large change in the ratio value will correspond to a small change in the position of L_{23}.

The customary solution to the first of these difficulties is to use a contrast stretching (actually compression) function. The commonly used ones are linear, cube-root, and logarithmic

$$y = K_1 x \,, \tag{8}$$

$$y = K_2 x^{1/3} \,, \tag{9}$$

$$y = K_3 \log x + K_4 \,. \tag{10}$$

Depending on the nature of the scene and the choices of constants, these schemes meet with varying degrees of success. We are proposing using the arctangent function,

$$y = k_5 \tan^{-1}(x) \,, \tag{11}$$

which, as we demonstrate below, has interesting properties. Figure 5 is a plot of these four stretching functions with the constants chosen so that the value of y was unity for X = 127, and the value of the logarithmic function was the average of the other functions at X = 1/127. This range of input values is based on the DN's for LANDSAT data.

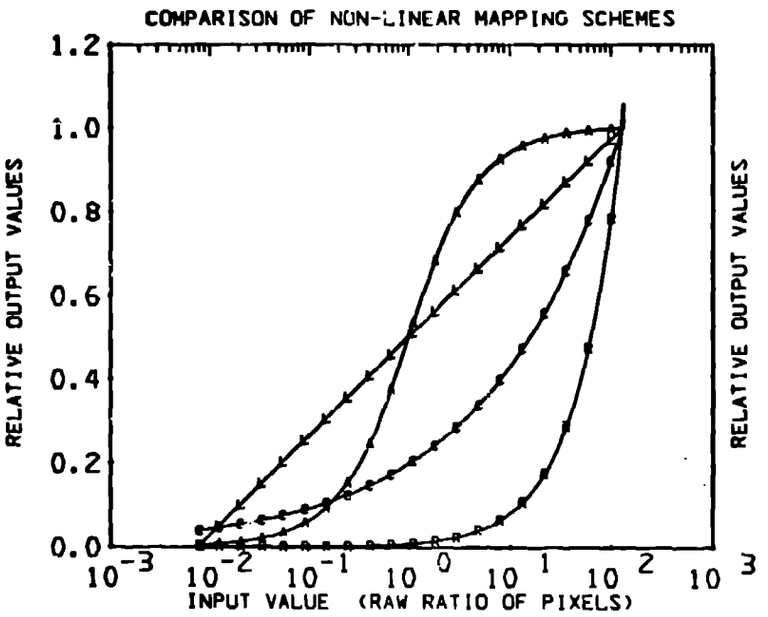

Fig. 5. Comparison of Contract Stretch Functions for Dynamic Range Reductions. All curves are normalized to produce an output of unity for an input of 127. Legend: A - arctangent, C - cube-root, L - Logarithm, R - direct ratio.

The arctangent transformation of a ratio image leads to an angle image. The two are equally valid specifications of the direction of the spectral signature line. Consider the projection L_{ij} of a signature line on the plane spanned by a pair of spectral bands as shown in Fig. 6.

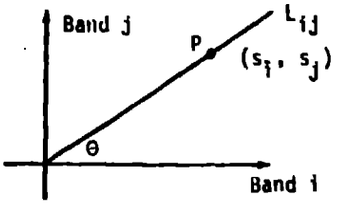

Fig. 6. the Motivation for the Angle Image The direction of the projection L_{ij} of the signature line is specified equally well by the inclination angle θ as by the slope, i.e., the ratio s_j/s_i.

The direction of line L_{ij} is specified equally well by the inclination angle θ as by the slope which is just the ratio s_j/s_i of Band j to Band i for points lying on L_{ij}. Most importantly, the range of θ is $[0, \pi/2]$. Thus we have the desirable dynamic range compression.

The angle image has a number of interesting properties. It contains the same information as the ratio image, i.e., the direction of the projection of the signature onto the plane of the two bands. If the two bands are interchanged, the new angle is just the complement of the old. This is analogous to forming the photographic negative of the original image. The angle picture is one in which the "distance" between signature lines is better represented by a Euclidean distance in the new space. This avoids the problem of changing sensitivity with the magnitude of the ratio. Finally, the arctangent stretching procedure is robust. By this we mean that it leads to acceptable displays of all ratio images from LANDSAT data. "Custom" choice of parameters for other stretching schemes may produce better displays of some regions of the ratio images, but the arctangent does not demand this sort of intervention.

The reason for this robustness lies in the nature of LANDSAT data. The bands are highly correlated; therefore, ratios near the value of unity should be most common. The angle picture uses most of its stretching range in the region about 1. The resemblance of the arctangent in Fig. 5 to the D-log E curve from photography should be noted. The ability of film, with these transfer characteristics, to record a wide dynamic range is well-known.

It seems that the arctangent of ratios of bands in multispectral imagery has a number of desirable and interesting properties. The efficacy of this approach in scene classification merits further investigation.

Comparison of Compression Schemes

In this section we compare the four compression schemes given in Equations 8-11. Plots of the transformations were given in Fig 5. In Fig. 5, we see that a linear compression does a very poor job of assigning gray levels to ratios for ratios less than unity. The cube root is a definite improvement, but it still assigns much of the data range to low gray levels. The arctangent and logarithm are quite similar except that greater contrast is assigned to ratios in the critical LANDSAT range of 1/5 to 5 by the arctangent than by the logarithm.

Ratio images of a portion of a LANDSAT frame covering the Los Alamos, NM area, using the four techniques for dynamic range compression described above are shown in Figures 7a through 7d. We are limited by space in this paper to displaying only the ratio of MSS Bands 4 to 7. Figure 8 shows the angle image of this ratio without correcting for the atmospheric bias.

The region shown in the photograph consists of a chain of 3.3 km mountains running from bottom to the top at the extreme left of the picture. In the center of the picture there is a plateau region cut by canyons with depths between 150 and 300 m. The Rio Grande river flows from upper right into a deep gorge and exits the frame at the bottom center. Four main vegetation regions are visible: dense fir and spruce forest on the mountain slopes, sparse piñon forest on the plateau, cottonwood groves along the river, and thinner piñon-juniper-grassland in the rolling terrain to the East (right) of the Rio Grande. Two small cities are visible in the center of the image, Los Alamos to the East of the mountains and White Rock to the West of the Rio Grande gorge.

The four stretching schemes discussed above were implemented as follows. The constants were chosen to map the spectral ratio range $[1/127, 127]$ into the range $[0., 1.]$. After applying these transformations, the data was clipped at the mean $\pm$ 2 standard deviations. The clipped data was then stretched to the range of the display device. The clipping had no effect on small ratios (dark pixels in the display) since 1/127 was within 2σ of the mean. No other stretching schemes were used, since the purpose of this demonstration is to show the robustness of using the arctangent. We acknowledge the fact that with scene dependent parameters every stretching scheme would perform better. One can see that the linear stretch does well in the regions of high ratio values (near the Rio Grande), that the cubic and logarithmic stretch do best at low densities. The arctangent seems to be adequate for all but the lowest densities.

A qualitative comparison of classification using these four transformations requires color photographs and cannot be given here.

References

1. Billingsley, F. C., Goetz, A. F. H., and Lindsley, J. N., "Color Differentiation by Computer Image Processing," Photogr. Sci. Eng., 14, pp. 28-35 (1970).

2. Yost, E., Anderson, R., and Goetz, A. F. H., "Isoluminous Additive Color Method for the Detection of Small Spectral Reflectivity Differences," Photogr. Sci. Eng., 17, pp. 177-182 (1973).

3. Rowan, L. C., Wetlaufer, P. H. Goetz, A. F. H., Billingsley, F. C., and Stewart, J. H., Discrimination of Rock Types and Detection of Hydrothermally Altered Areas in South-Central Nevada by the Use of Computer-Enhanced ERTS Images, Geological Survey Professional Paper, U. S. Government Printing Office, 1974.

4. Goetz, A. F. H., Billingsley, F. C., Gillespie, A. R., Abrams, M. J., Squires, R. L., Shoemaker, E. M., Luchitta, I., and Elston, D. P., "Application of ERTS Images and Image Processing to Regional Geologic Problems and Geologic Mapping in Northern Arizona," JPL Technical Report 32-1597, 1975.

5. Berlin, G. L., Chavez, P. S., Grow, T. E., and Soderblom, L. A., "Preliminary Geologic Analysis of Southwest Jordan from Computer Enhanced LANDSAT I Image Data," Proc. Am. Soc. of Photogrammetry, pp. 545-563, 1976.
6. Lansing, J. C., Jr. and Cline, R. W., "The Four- and Five-Band Multispectral Scanners for LANDSAT," Optical Eng. 14, p. 318, 1975
7. Friedman, B., Principles and Techniques of Applied Mathematics, Chap. 1, pp. 28-29, John Wiley & Sons, 1956.
8. Siegal, B. S. and Abrams, M. J., "Geologic Mapping Using LANDSAT Data," Photogrammetric Eng. and Remote Sensing, 42, 1976.
9. Duda, R. O. and Hart, P. E., Pattern Classification and Scene Analysis, Chap. 9, pp. 332-335, John Wiley and Sons, 1973.
10. Chavez, P. S., Jr., "Atmospheric, Solar, and M.T.F. Corrections for ERTS Digital Imagery," Proceedings, American Society of Photogrammetry, pp. 69-69a, 1975.

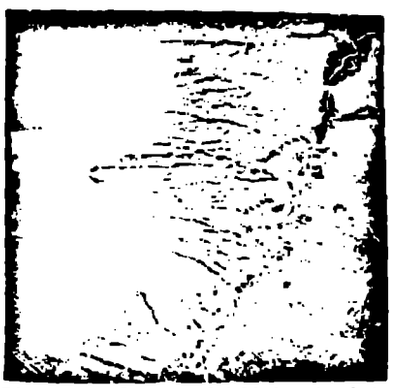

Fig. 7a. Ratio of MSS bands 4 to 7. Linearly stretched.

Fig. 7b. Ratio of MSS bands 4 to 7. Cube root stretch.

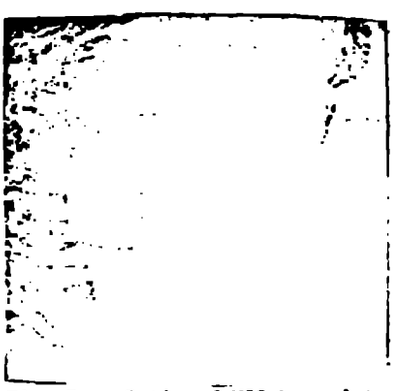

Fig. 7c. Ratio of MSS bans 4 to 7. Logarithmic stretch.

Fig. 7d. Ratio of MSS bands 4 to 7. Arctangent stretch.

Fig. 8. Ratio of MSS bands 4 to 7 with no correction for atmospheric bias. Arctangent stretch.